Algorithm for Decomposition of Additive Strain from Dense Network of Thin Film Sensors

Hussam Saleem[1], Austin Downey[1,3], Simon Laflamme[1,2]
[1] Dept. of Civil, Constr., and Env. Engineering, Iowa State University, Ames, IA, USA;
[2] Dept. of Electrical and Computer Engineering, Iowa State University, Ames, IA, USA;
[3] Dept. of Wind Energy Science Engineering and Policy, Ames, Iowa State University, IA, USA;

ABSTRACT

The authors have developed a capacitive-based thin film sensor for monitoring strain on mesosurfaces. Arranged in a network configuration, the sensing system is analogous to a biological skin, where local strain can be monitored over a global area. The measurement principle is based on a measurable change in capacitance provoked by strain. In the case of bi-directional in-plane strain, the sensor output contains the additive measurement of both principal strain components. In this paper, we present an algorithm for retrieving the directional strain from measurements. The algorithm leverages the dense network application of the thin film sensor to reconstruct the surface strain map. A bi-directional shape function is assumed, and it is differentiated to obtain expressions for planar strain. A least square estimator (LSE) is used to reconstruct the planar strain map from the sensors measurement's, after the system's boundary conditions have been enforced in the model. The coefficients obtained by the LSE can be used to reconstruct the estimated strain map or the deflection shape directly. Results from numerical simulations and experimental investigations show good performance of the algorithm, in particular for monitoring surface strain on cantilever plates.

Keywords: structural health monitoring, capacitive-based sensor, flexible membrane sensor, sensor network, signal decomposition.

1 INTRODUCTION

Structural health monitoring (SHM) of mesosystems such as transportation infrastructures, aerospace structures, and energy systems, is a difficult task, due to the large geometrical size of the monitored systems.[1] Existing sensing solutions are typically limited on a technological perspective, where linking signals to condition assessment is very complex, and/or on an economic perspective, where large-scale deployments is hard to financially justify. Due to the important potential benefits of SHM to management of operation and maintenance programs of mesosystems, there is a need to develop scalable sensing solutions enabling automatic condition assessment.[2]

The authors proposed a novel sensing technology specifically designed to be highly scalable. It consists of soft elastomeric capacitor (SEC), fabricated from an inexpensive nanocomposite customizable in shapes and sizes.[3,4] The sensing principle is based on a change in geometry in the SEC that can be measured as a change in the capacitance. Arranged in a network configuration, the sensing technology can measure discrete deformations over a large area, analogous to biological skin. Others have proposed such skin-type sensors.[5–7] In particular, capacitive-based technologies include applications to humidity, pressure, strain, and tri-axial measurements.[8–12]

Sensors and Smart Structures Technologies for Civil, Mechanical, and Aerospace Systems 2015,
edited by Jerome P. Lynch, Kon-Well Wang, Hoon Sohn, Proc. of SPIE Vol. 9435, 94351N
 · doi: 10.1117/12.2084369

A particular feature of the SEC is its bi-directional strain measurement capabilities, where its signal measures the additive in-plane strain. While this could be an advantage in vibration-based monitoring as shown in Ref.,[13] the utilization of the SEC as a strain sensor necessitates the decomposition of its signal into strain components. In this paper, the authors present an algorithm enabling such decomposition. The strategy consists of leveraging the dense network configuration of the SEC, imposing a strain map, and computing the regression coefficients after enforcement of the boundary conditions.

This paper is organized as following. Section 2 presents the background on the technology, which includes the fabrication method and the electromechanical model. Section 3 validates the electromechanical model for both quasi-static and dynamic loads. Section 4 describes the strain decomposition algorithm and conducts its validation experimentally and via numerical simulations. Section 5 concludes the paper.

2 Background

2.1 Fabrication Method

The fabrication process of the SEC is as follows. First, poly-styrene-ethylene-butadiene-styrene (SEBS, Mediprene Dryflex) is dissolved into toluene. Second, the resulting solution is mixed with 15 vol% of titanium dioxide (titania or TiO_2, Sachtleben R 320 D) nanoparticles to increase the materials' robustness and permittivity. Third, the particles are uniformly dispersed within the polymer matrix using a sonic dismembrator (Fisher Scientific Model 120 Sonic Dismembrator) for 10 minutes. Fourth, the resulting solution is cast onto a 80×80 mm^2 flat glass plate to create the dielectric. Fifth, during the drying of the dielectric mix, another SEBS solution is mixed with a 10 vol% concentration of carbon black (CB) particles, and sonicated in a sonication bath for 6 hours. Finally, the conductive mix is painted on the top and bottom surfaces of the dried dielectric to create the compliant electrodes. During the drying process of the electrodes, copper tape is embedded in the SEBS+CB mix to create the physical connection to the DAQ. Fig. 1a is a picture of the resulting SEC.

2.2 Electro-Mechanical model

The SEC is designed to be adhered onto the monitored surface along its $x-y$ plane (Fig. 1b). Assuming low frequency measurements (< 1 kHz), the transducer can be considered as a non-lossy capacitor with capacitance C

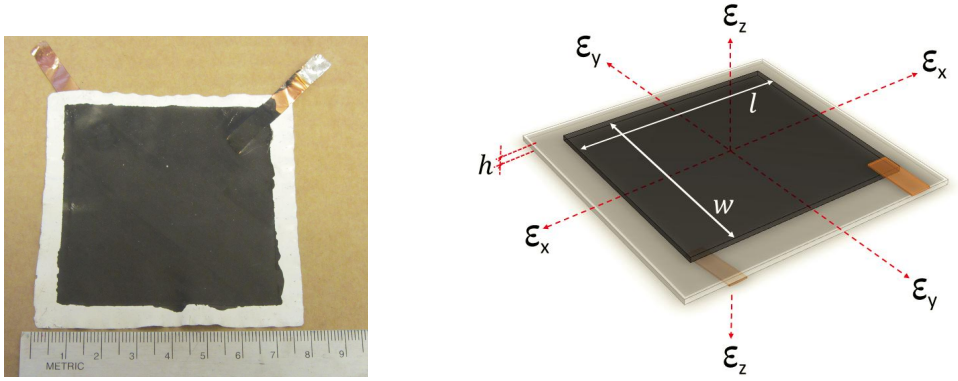

(a) single SEC (80×80 mm^2) (b) reference axes

Figure 1: a soft elastomeric capacitor (SEC)

$$C = e_0 e_r \frac{A}{h} \tag{1}$$

where $e_0 = 8.854$ pF/m is the vacuum permittivity, e_r is the polymer relative permittivity, A is the area of the sensor area of width w and length l, and h is the thickness of the dielectric. Assuming small strain, one can take the differential of Eq. (1)

$$\frac{\Delta C}{C} = \left(\frac{\Delta l}{l} + \frac{\Delta w}{w} - \frac{\Delta h}{h} \right) = \varepsilon_x + \varepsilon_y - \varepsilon_z \tag{2}$$

where ε_x, ε_y and ε_z are strains in the x, y and z directions as shown in Fig. 1b(b). An expression relating ε_z to ε_x and ε_y can be obtained using Hooke's law for in-plane stress

$$\varepsilon_z = -\frac{\nu}{1-\nu}(\varepsilon_x + \varepsilon_y) \tag{3}$$

The final form of the electromechanical model is obtained by integrating Eq. (3) in Eq. (2)

$$\frac{\Delta C}{C} = \lambda(\varepsilon_x + \varepsilon_y) \tag{4}$$

where $\lambda = \frac{1}{1-\nu}$ represents the gauge factor of the sensor. For SEBS, $\nu \approx 0.49$,[14] which gives a gauge factor $\lambda \approx 2$.

3 Experimental Validation

In this section, the electromechanical model is validated experimentally in order to support the methodology used in the numerical simulations. First, a quasi-static load test is conducted on a fiber-glass plate to experimentally validate Eq. (4). Second, a dynamic characterization is conducted to demonstrate that the electromechanical model holds for structural responses under 15 Hz.

3.1 Quasi-Static Load Test

The experimental setup for the quasi-static load test consists of six SECs deployed on a cantilever fiberglass plate of dimensions of dimensions 416 $\times$ 324 $\times$ 4 mm^3. The number of sensors is limited by the capacity of the data acquisition system used herein to read the SEC signals. Resistive strain gauges (RSGs) of 1 $\mu\varepsilon$ resolution (Vishay Micro-Measurements, CEA-06-500UW-120) are deployed around each SEC to benchmark the results. Two load configurations are investigated at the free edge: 1) at the center; and 2) at the corner (top-right in Fig. 4b). Data from the SECs are acquired using an off-the-shelf data acquisition system (ACAM PCap01) recorded at 20 Hz. Data from the RGSs are measured using a Hewlett-Packard 2850 data acquisition system at a sampling frequency of 1.7Hz. Fig. 2 shows the experimental setup.

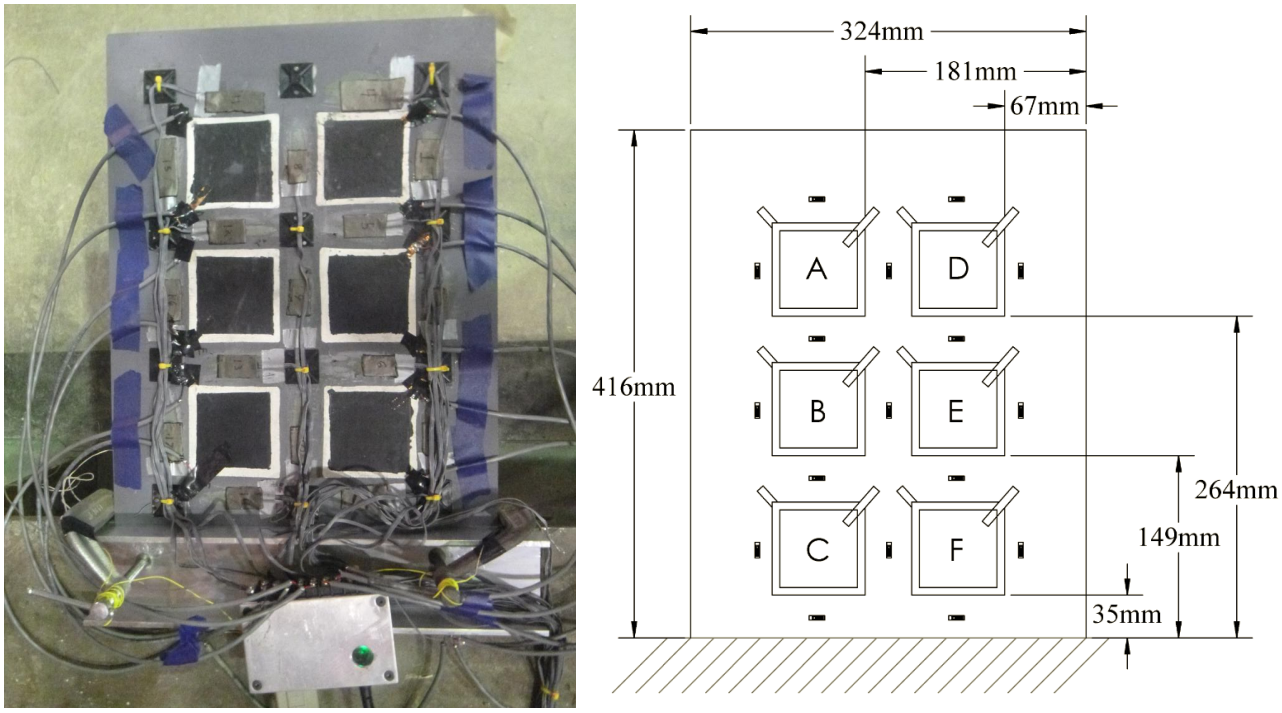

Figure 2: quasi-static test setup

Fig.3 shows the time series results for the recorded additive strain from the SECs and RSGs. The additive strain from the SECs is directly obtained from Eq. (4), and compared against the average additive measurements of the RSGs surrounding the SECs. Plots show five distinct plateaus of strain. The first three plateaus are used for sensor calibration, and the fourth and fifth plateaus represent results from the center and the corner loads, respectively. SECs A and D exhibit a higher variance with respect to other SECs, which can be explained by the lower level of strain resulting in a higher noise-to-signal ratio. Note that it was reported in previous work that the accuracy of an SEC in this particular measurement configuration is 25 $\mu\varepsilon$.[3] Results show good agreement between the SECs strain readings, obtained from the electromechanical model, and the RSGs.

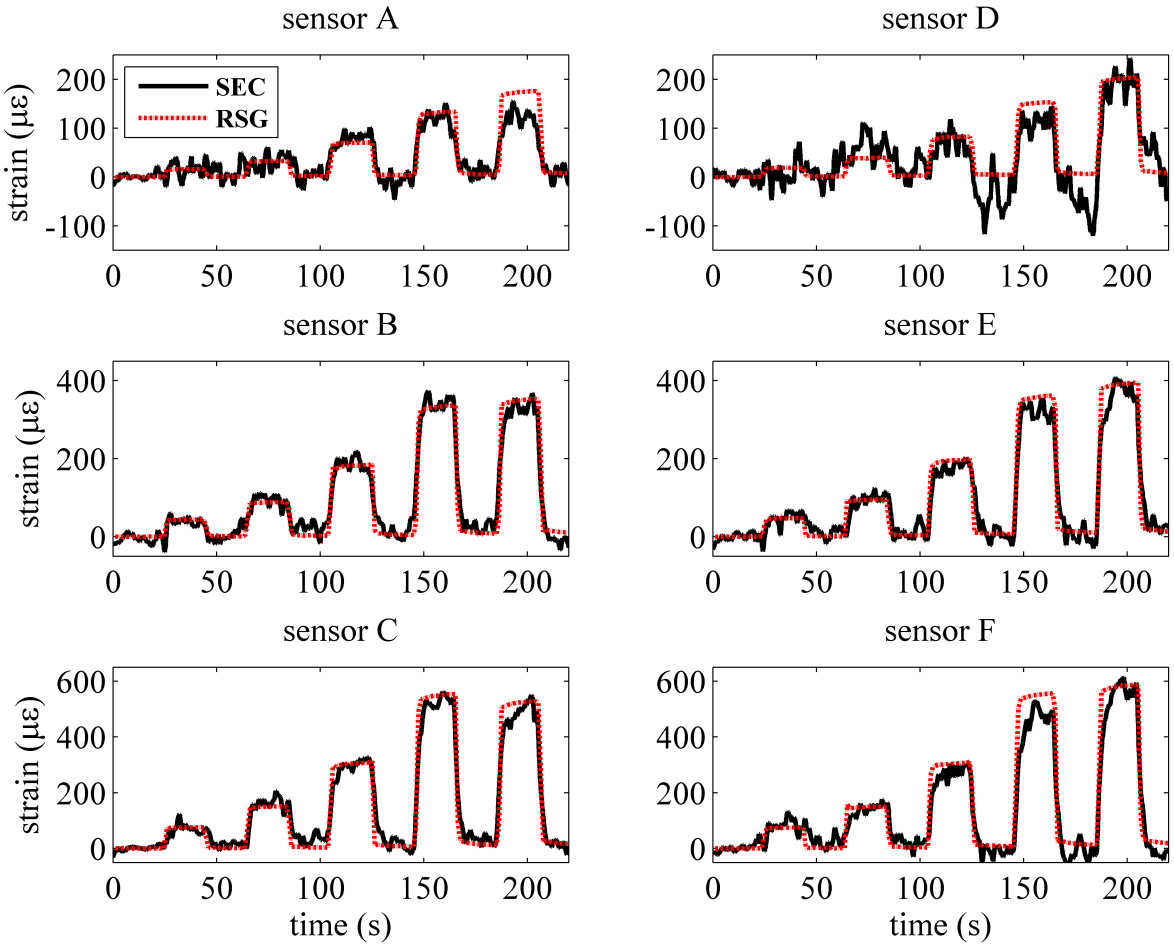

Figure 3: static test results

3.2 Dynamic Characterization

The SEC was subjected to a dynamic load to evaluate the linearity of the electromechanical model for typical structural responses under 15 Hz. The test setup, shown in Fig. 4a, consisted of adhering three SECs onto the top surface of an aluminum plate, and subjecting the plate to an axial load. RSGs were adhered onto the bottom surface of the plate to verify the SEC signal. The axial load was a low amplitude harmonic load ranging from 1 Hz to 15 Hz in increments of 1 Hz. The same data acquisition method as for the quasi-static test was used. The gauge factors of the SECs at each frequency was back-calculated using Eq.(4), and taking $\varepsilon_y = -\nu_m \varepsilon_x$, where ν_m is the Poisson ratio of the aluminum plate, taken as $\nu_m = 0.33$.

Figure 4(b) shows the experimental gauge factor from an SEC as a function of the frequency. The gauge factor remains approximately constant over the range 1-15 Hz, which confirms that the electromechanical model can be used to measure dynamic strain over a dynamic range corresponding to typical structural responses.

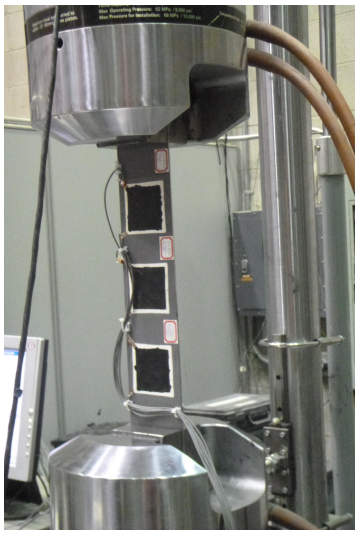

(a)

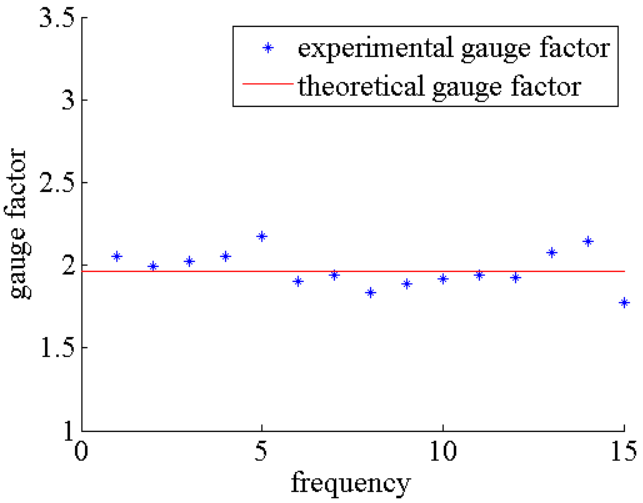

(b)

Figure 4: (a) test setup and (b) experimental gauge factor

4 Strain Decomposition Algorithm

In this section, the strain decomposition algorithm is presented and validated experimentally and via numerical simulations.

4.1 Algorithm formulation

The strain decomposition algorithm starts by assuming a smooth deflection function (n^{th} order polynomial) based on Kirchhoff plate theory. Consider plate with lengths L_x, width L_y and thickness c, with an assumed deflection shape of the type

$$\begin{aligned} w(x,y) &= \sum_{i=0,j=0}^{n} a_{ij} x^i y^j \\ &= \mathbf{HA} \end{aligned} \tag{5}$$

where w is the deflection, and a_{ij} are coefficients, $\mathbf{A}$ is the coefficient vector, and $\mathbf{H}$ is the sensor location vector. Expressions for strains ε_x and ε_y can be directly derived from Eq. (5)

$$\begin{aligned} \varepsilon_x(x,y) &= -\frac{c}{2}\frac{\partial^2 w}{\partial x^2} = \mathbf{H}_x\mathbf{A}_x \\ \varepsilon_y(x,y) &= -\frac{c}{2}\frac{\partial^2 w}{\partial y^2} = \mathbf{H}_y\mathbf{A}_y \end{aligned} \tag{6}$$

The signal S_m of the mth SEC can be written in terms of a total strain ε_t

$$S_m = \varepsilon_{t,m} = \varepsilon_{x,m} + \varepsilon_{y,m} \tag{7}$$

where S_m is pre-divided by the gauge factor λ for clarity. The SEC signals can be represented in matrix notation using Eq. (6):

$$\begin{aligned}\mathbf{S} &= \left[\begin{array}{c|c} \mathbf{H}_x & \mathbf{H}_\mathbf{y} \end{array}\right] \left[\frac{\mathbf{A}_x}{\mathbf{A}_y}\right] \\ &= \mathbf{H}_{xy}\mathbf{B}\end{aligned}$$

where $\mathbf{S}$ is the SEC signal vector. An estimate for $\mathbf{B}$ is obtained using an LSE

$$\hat{\mathbf{B}} = (\mathbf{H}_{xy}^T\mathbf{H}_{xy})^{-1}\mathbf{H}_{xy}^T\mathbf{S} \tag{8}$$

where the hat indicates an estimation. In this particular configuration, $\mathbf{H}_{xy}$ is collinear and $\mathbf{H}_{xy}^T\mathbf{H}_{xy}$ singular. To remove collinearity in $\mathbf{H}_{xy}$, boundary conditions are assumed and enforced directly in the matrix. For instance, in the case of a cantilever plate, the following boundary conditions can be assumed:

1. $\varepsilon_y(0, a_y \leq y \leq L_y - a_y) = 0$;
2. $\varepsilon_y\left(a_x \leq x \leq L_x - a_x, 0\right) = \varepsilon_y\left(a_x \leq x \leq L_x - a_x, L_y\right) = -\nu_m\varepsilon_x$;
3. $\varepsilon_x(L_x, a_y \leq y \leq L_y - a_y) = -\nu_m\varepsilon_y$

where ν_m is the Poisson ratio of the monitored material, a_y and a_x are positive constants such that $0 \leq a_x \leq L_x$ and $0 \leq a_y \leq L_y$ to account for different boundary conditions at corners. After enforcing the boundary conditions and obtaining the estimate $\hat{B}$, expressions for estimated strains are taken as

$$\hat{\varepsilon}_x = \mathbf{H}_{xy}\mathbf{A}_x \qquad \hat{\varepsilon}_y = \mathbf{H}_{xy}\mathbf{A}_y \tag{9}$$

4.2 Experimental Validation

The algorithm is first validated on data from the experimental investigation discussed in the previous section (Fig. 3). Due to the small number of sensor nodes (6), only two sensors were used for the boundary conditions (sensors C and F) with the assumption $\varepsilon_y = 0$. The deflection shape $w(x, u)$ was assumed to follow a fourth order polynomial in the x direction, and third order polynomial in the y direction. The corner load case is used for this validation due to the asymmetry in its response.

Table I lists the strain decomposition results, comparing the estimated values (denoted by a hat) and experimental values measured by the RSGs. Note that the RSG values are taken as the average of the two RSGs surrounding an SEC in a particular direction. Results show an overall acceptable performance of the algorithm and demonstrates the promise of the algorithm at decomposing principal strain components. Larger discrepancies can be explained by 1) the signal-to-noise ratio in the SEC signal, which is notably observable in Fig. 4 for sensor D; 2) the weak assumption on the boundary condition for sensors C and F, in particular for the center load case; and 3) the low number of sensors used in the experiment, which limits the application of a consistent polynomial and additional boundary conditions.

Table I: Algorithm output

sensor	ε_x	$\widehat{\varepsilon}_x$	$\lvert\varepsilon_x - \widehat{\varepsilon}_x\rvert$	ε_y	$\widehat{\varepsilon}_y$	$\lvert\varepsilon_y - \widehat{\varepsilon}_y\rvert$
A	136	186	49.5	38.2	-11.6	49.8
B	342	340	1.90	9.74	10.9	1.14
C	534	543	8.69	0.65	0.00	0.65
D	166	385	220	37.1	-178	215
E	374	465	91.0	19.2	-77.2	96.4
F	590	593	3.48	-5.56	0.00	5.56

4.3 Simulation

The algorithm performance is demonstrated via numerical simulations one a fiber-glass plate as shown in Fig.5. A dense array of 11 $\times$ 11 SECs is simulated, with spacings of 3.8 mm side-to-side in both directions. A corner load of 1.5 N is applied on the plate to create a non-uniform deflection shape. All of the perimeter sensors are used as boundary condition sensors using the assumptions listed above with $a_x = a_y = 0$. These sensors are shown as red squares in Fig.5. The decomposition is done using a 5^{th} order polynomial ($n = 5$).

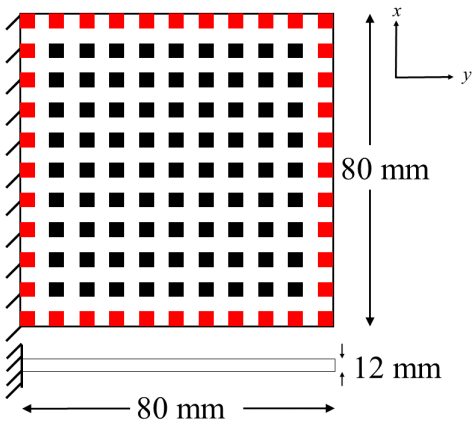

Figure 5: simulated system; squares indicate SECs

Fig. 6 shows the estimated strain in both directions, where the fixity is along the y-axis at $x = 0$. Fig. 8 is two dimensional representation of the absolute percentage error (APE) at various locations. Results show good estimation for ε_x with an average absolute error of 26%, with the largest fitting error located at the free edge. The fitting error is larger for ε_y, with an average absolute error of 86%. The APE$_y$ exhibits larger error both at the fixed and free edges. The larger error along the y-axis can be attributed to higher dependence of ε_y on the assumptions on boundary conditions. Nevertheless, the resulting deflection shape, showed in Fig. 7, exhibits a good fit, with a mean absolute error of 26%. This good performance despite the larger fitting error on ε_y is explained by the lower magnitude of ε_y with respect to ε_x.

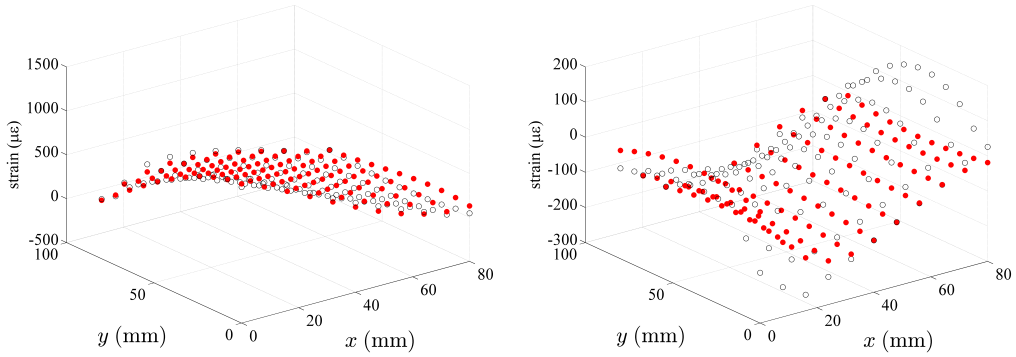

(a) ε_x (b) ε_y

Figure 6: estimated strain (filled red circles) vs analytical strain (black circles)

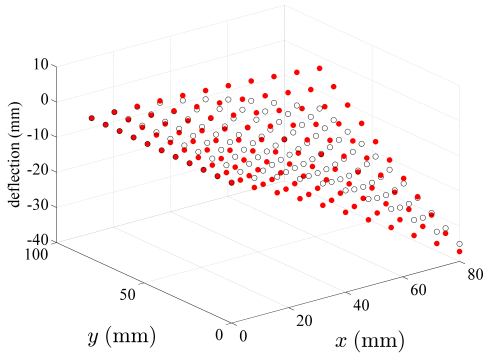

Figure 7: estimated deflection (filled red circles) vs analytical deflection (black circles)

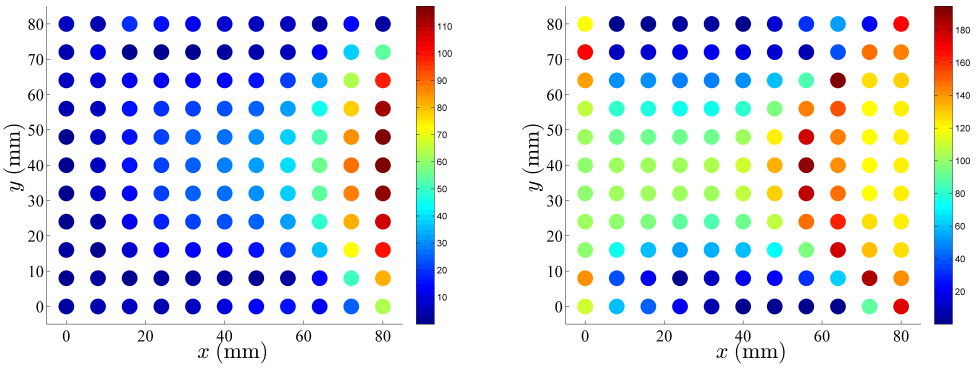

(a) APE_x (b) APE_y

Figure 8: simulation results of the plate (a)APE_x and (b)APE_y

5 Conclusion

We have presented a novel thin film sensor, the SEC, is specifically designed to monitor mesosurfaces. An electromechanical model for the SEC was presented and experimentally validated with static and dynamic excitations. The linearity of the model was validated over the range 1-15 Hz. A particular feature of the SEC is its bi-directional strain measurement capabilities, where its signal measures the additive in-plane strain. An algorithm was developed to leverage a dense network application, and decompose the signal into principal strain components. The algorithm was validated using experimental results and demonstrated with numerical simulations on a plate subjected to an asymmetric load. Results show good performance for the strain fit along the major strain component, and provided a good fit for the deflection shape. It was found that the performance of the algorithm is strongly dependent on the assumptions on the boundary conditions.

Results presented in this paper show the promise of the technology at monitoring large-scale surfaces, such as wind turbine blades and aircraft wings. For example, it could be used to extract discrete information on a global surface, such as local damage. An SEC network could also be used to extract strain maps and deflection shapes. Such information could be integrated directly into a condition assessment model to enable condition-based maintenance.

Acknowledgements

The development of the SEC technology is supported by grant No. 1001062565 from the Iowa Alliance for Wind Innovation and Novel Development and grant No. 13-02 from the Iowa Energy Center. Their support is gratefully acknowledged.

REFERENCES

[1] S. Laflamme, F. Ubertini, H. Saleem, A. DAlessandro, A. Downey, H. Ceylan, A. L. Materazzi, Dynamic characterization of a soft elastomeric capacitor for structural health monitoring, Journal of Structural Engineering.

[2] P. C. Chang, A. Flatau, S. C. Liu, Review paper: Health monitoring of civil infrastructure, Structural Health Monitoring 2 (3) (2003) 257–267.

[3] S. Laflamme, H. Saleem, B. Vasan, R. Geiger, D. Chen, M. Kessler, K. Rajan, Soft elastomeric capacitor network for strain sensing over large surfaces, Mechatronics, IEEE/ASME Transactions on 18 (6) (2013) 1647–1654.

[4] S. Laflamme, M. Kollosche, J. J. Connor, G. Kofod, Robust flexible capacitive surface sensor for structural health monitoring applications, Journal of Engineering Mechanics 139 (7) (2012) 879–885.

[5] L. Gao, E. T. Thostenson, Z. Zhang, J.-H. Byun, T.-W. Chou, Damage monitoring in fiber-reinforced composites under fatigue loading using carbon nanotube networks, Philosophical Magazine 90 (31-32) (2010) 4085–4099.

[6] I. Kang, M. J. Schulz, J. H. Kim, V. Shanov, D. Shi, A carbon nanotube strain sensor for structural health monitoring, Smart Materials and Structures 15 (3) (2006) 737.

[7] R. K. Srivastava, V. S. M. Vemuru, Y. Zeng, R. Vajtai, S. Nagarajaiah, P. M. Ajayan, A. Srivastava, The strain sensing and thermalmechanical behavior of flexible multi-walled carbon nanotube/polystyrene composite films, Carbon 49 (12) (2011) 3928 – 3936.

[8] H. P. Hong, K. H. Jung, N. K. Min, Y. H. Rhee, C. W. Park, A highly fast capacitive-type humidity sensor using percolating carbon nanotube films as a porous electrode material, in: Sensors, 2012 IEEE, 2012, pp. 1–4.

[9] D. J. Lipomi, M. Vosgueritchian, B. C. K. Tee, S. L. Hellstrom, J. A. Lee, C. H. Fox, Z. Bao, Skin-like pressure and strain sensors based on transparent elastic films of carbon nanotubes, Nature Nanotechnology 6 (12) (2011) 788–792.

[10] K. Arshak, D. McDonagh, M. Durcan, Development of new capacitive strain sensors based on thick film polymer and cermet technologies, Sensors and Actuators A: Physical 79 (2) (2000) 102 – 114.

[11] M. Suster, J. Guo, N. Chaimanonart, W. Ko, D. Young, A high-performance mems capacitive strain sensing system, Microelectromechanical Systems, Journal of 15 (5) (2006) 1069–1077.

[12] J. A. Dobrzynska, M. A. M. Gijs, Polymer-based flexible capacitive sensor for three-axial force measurements, Journal of Micromechanics and Microengineering 23 (1) (2013) 015009.

[13] F. Ubertini, S. Laflamme, H. Ceylan, A. L. Materazzi, G. Cerni, H. Saleem, A. DAlessandro, A. Corradini, Novel nanocomposite technologies for dynamic monitoring of structures: a comparison between cement-based embeddable and soft elastomeric surface sensors, Smart Materials and Structures 23 (4) (2014) 045023.

[14] A. Wilkinson, M. Clemens, V. Harding, The effects of sebs-g-maleic anhydride reaction on the morphology and properties of polypropylene/pa6/sebs ternary blends, Polymer 45 (15) (2004) 5239 – 5249.